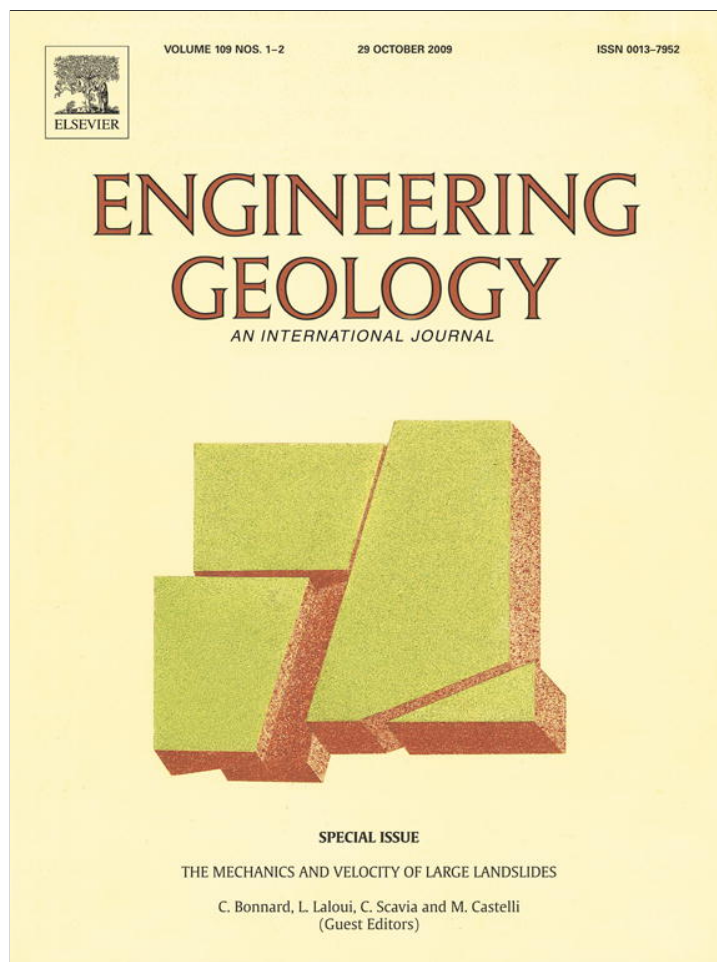


Provided for non-commercial research and education use.
Not for reproduction, distribution or commercial use.



This article appeared in a journal published by Elsevier. The attached copy is furnished to the author for internal non-commercial research and education use, including for instruction at the authors institution and sharing with colleagues.

Other uses, including reproduction and distribution, or selling or licensing copies, or posting to personal, institutional or third party websites are prohibited.

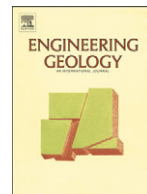
In most cases authors are permitted to post their version of the article (e.g. in Word or Tex form) to their personal website or institutional repository. Authors requiring further information regarding Elsevier's archiving and manuscript policies are encouraged to visit:

<http://www.elsevier.com/copyright>



Contents lists available at ScienceDirect

Engineering Geology

journal homepage: www.elsevier.com/locate/enggeo

Geophysical investigation of a large landslide in glaciolacustrine clays in the Trièves area (French Alps)

D. Jongmans^{a,*}, G. Bièvre^{a,b}, F. Renalier^a, S. Schwartz^a, N. Bearez^b, Y. Orengo^a

^a LGIT, Maison des Géosciences, Université Joseph Fourier, BP 53, 38041 Grenoble Cedex 9, France

^b CETE Lyon, LRPC Autun, BP 141, 71404 Autun cedex, France

ARTICLE INFO

Article history:

Received 11 December 2007

Received in revised form 6 October 2008

Accepted 9 October 2008

Available online 1 November 2008

Keywords:

Landslide

Clay

Geophysical prospecting

ABSTRACT

Slope movements in clay deposits are spread all over the world and result from complex deformation processes, including internal strains in the landslide body and slipping along rupture surfaces. Such mass movements are likely to generate changes in the geophysical parameters characterizing the ground, which can be used to map the landslide body. In the last decade, geophysical techniques have been increasingly used for landslide investigation purposes. However, the success of any geophysical technique is overall controlled by the existence of a geophysical contrast differentiating the body to be mapped. For landslides affecting thick clay materials (from soft clay to shale or marl), electrical and seismic techniques have been mainly applied in the past. In this study, we attempt to physically characterize the deformation within a large slide (Avignonet) affecting laminated clays which were deposited in a glacially dammed lake during the Würm period. Clay deposits, which cover an area of 300 km² south of Grenoble (French Alps) and have a maximum thickness of 200 m, overlay compact alluvial layers and marly limestone of Mesozoic age. Piezometric data at Avignonet show that the water table is very shallow, implying that the slide developed in saturated clay. Several seismic and electrical profiles were performed in order to tentatively correlate the variations of P-wave (V_p) velocity, S-wave velocity (V_s) and electrical resistivity with geotechnical data and morphological observations. In such saturated and fine material, it turned out that only the S-wave velocity exhibits significant variations with the displacement rates and the morphological features. V_s values at shallow depth were found to be inversely correlated with displacement rates measured by GPS, with a division by at least a factor of 2 between the zones unaffected and strongly deformed by the landslide. These results suggest that V_s mapping could provide valuable information on the deformation state of the clay material and that the evolution of V_s with time could be used as an indicator for characterizing the landslide activity in the subsurface, including the evolution into a flow.

© 2008 Elsevier B.V. All rights reserved.

1. Introduction

The Trièves area (French Alps) is covered by Quaternary clays with a maximum thickness of 200 m, which were deposited in a glacially dammed lake during the Würm period (Monjuvent, 1973). These clay deposits are affected by numerous deep landslides which can evolve into mudflows. Slope movements in such fine grained soils are found worldwide and usually result from complex deformation processes, including internal strains in the landslide body and slipping along rupture surfaces (see Picarelli, 2000 and Picarelli et al., 2004). Such mass movements are likely to generate changes in the geophysical parameters characterizing the ground, which can be used to map the landslide body. Since the pioneering work of Bogoslovsky and Ogilvy (1977), geophysical techniques have been increasingly but relatively little used (or referenced) for landslide investigation purposes. A review of the application of geophysical techniques to landslide

investigation was recently published (Jongmans and Garambois, 2007). Among the reasons explaining the reluctance to employ geophysical techniques, one can mention the relative difficulty of deploying geophysical layouts (although the expense is far less than the one required for drilling), the limitations of earlier geophysical methods to adequately investigate a 3D structure, and the problem of linking the measured geophysical parameters to geotechnical properties. Over the last fifty years, since the pioneering works of Archie (1942) and Willye et al. (1956) an enormous effort has been made in petroleum exploration to understand, both theoretically and experimentally, the relations between geophysical parameters (e.g. seismic P- and S-wave velocities, resistivity and permittivity) and rock mass properties (for a review, see for instance Mavko et al., 2003). In clay material specifically, Mondol et al. (2007) recently studied the changes in geophysical properties during burial through experimental tests on dry and brine saturated clay aggregates from smectite to kaolinite. In saturated samples, V_p values were shown to be sensitive to the vertical effective stress, increasing on average from 1500 m/s at 5 MPa to 2350 m/s at 50 MPa. V_s values exhibit the same tendency but

* Corresponding author.

E-mail address: denis.jongmans@ujf-grenoble.fr (D. Jongmans).

with a far greater variation, from 300 m/s to almost 850 m/s for the same stress values. At shallow depth, Leucci and De Giorgi (2006) investigated the effects of fracture on P and S wave velocity values in sedimentary rocks. They experimentally showed that, if the two seismic velocities significantly decrease with the fracturing intensity, V_s is more sensitive to fracture parameters. These two studies, among many others, illustrate that geophysical parameters can be of interest for characterizing ground mechanical properties like the compactness or the degree of fracturing.

The recent emergence of 2D and 3D geophysical imaging techniques, easy to deploy on slopes and investigating a large volume in a non-invasive way, has made geophysical methods more attractive for landslide applications. However, the success of any geophysical campaign depends on four main controlling factors (McCann and Forster, 1990): a) the existence of geophysical contrasts within the body to be mapped, b) the resolution and penetration of the applied methods, c) the calibration of geophysical techniques by geological or geotechnical data and d) the signal to noise ratio. In the case of landslides affecting thick clayey deposits (from soft clay to shale or marl), electrical (Caris and van Asch, 1991; Schmutz et al., 2000; Lapenna et al., 2005; Méric et al., 2007) and seismic methods (Caris and van Asch, 1991; Grandjean et al., 2006; Méric et al., 2007) have been mostly used in the past. In compact clays and marls, landslide bodies are associated with low resistivity values (generally between 10 and 30 Ω m) while the unaffected ground is characterized by a resistivity over 60–75 Ω m (Caris and van Asch, 1991; Schmutz et al., 2000; Lapenna et al., 2005). Dislocation of material by the slide allows the weathering of the minerals and the water content to be increased, lowering the resistivity values in the landslide body. As the motion and the resulting internal strains can alter the compactness of the moving mass, seismic methods usually show a contrast in seismic velocity (P-wave or S-wave) between the slide and the unaffected ground. Applying the seismic refraction technique on a small landslide in black marl material (French Alps), Caris and van Asch (1991) found a strong P-wave velocity contrast between the landslide body (350 m/s) and the bedrock (2800 m/s) which varies in depth between 4 and 9 m. Méric et al. (2007) derived S-wave velocity profiles on two landslides in clayey materials, from the inversion of surface waves (Wathelet et al., 2004). In both cases, a large contrast of V_s was detected between the sliding (250–300 m/s) and the stable mass (550–800 m/s) at depths varying between 20 and 35 m, in agreement with other geophysical data and borehole measurements. The H/V technique (Nakamura, 1989), which measures the fundamental frequency of the site, was applied on clayey landslides (Gallipoli et al., 2000; Méric et al., 2007) for estimating the depth of the rupture surface assuming a constant V_s value within the slide. This quick and easy to interpret technique can however yield inaccurate results in case of severe 2D and 3D effects (Guillier et al., 2006).

The aim of this study is to test the ability of the three geophysical parameters electrical resistivity, P-wave velocity and S-wave velocity to distinguish and characterize the deformation generated by the Avignonet landslide consisting of saturated laminated clays. Five different geophysical methods (seismic noise measurement, electrical resistivity tomography, P-wave seismic refraction tomography, S-wave seismic refraction tomography and surface wave inversion) were applied along a profile where geotechnical data (borehole logs, inclinometer data, GPS measurements) are available. Comparison of the two sets of data suggests that the S-wave velocity is the most sensitive parameter to gravitational deformation in such kind of deposits.

2. Geological and geotechnical contexts

The Trièves region is located 40 km south of the city of Grenoble in the western Alps (Fig. 1). Morphologically, this area is a large depression of about 300 km², which is drained by the Drac River and

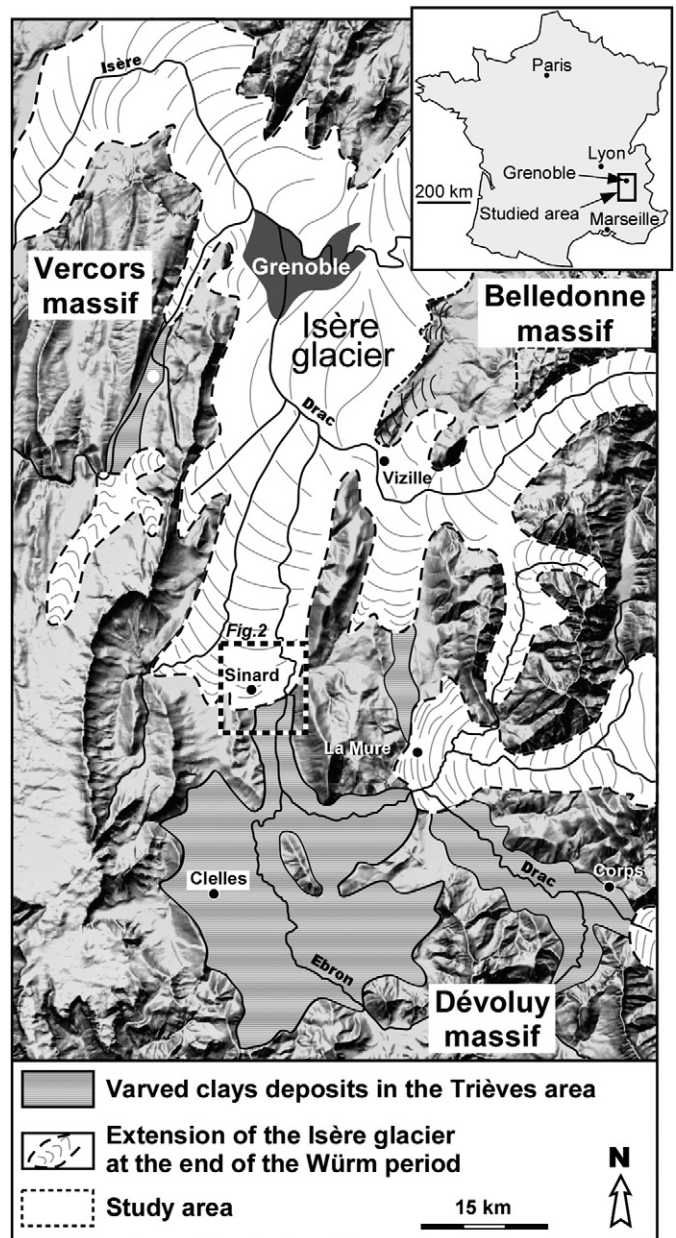


Fig. 1. Location map of Grenoble and the Trièves region, showing the varved clay deposits and the extension of the glaciers at the end of the Würm period. The studied area is indicated with a box (dashed bold line).

its tributaries. It is limited to the West and South by the Vercors and the Dévoluy carbonate massifs, respectively, and to the East, by the dome structure of La Mure (Fig. 1). During the last maximum glacial extension (Würm period, –45 000 years), the Isère glacier blocked downstream the torrential flows coming from the South (Fig. 1) generating an ice-dammed lake (Monjuvent, 1973). This lake progressively invaded the whole zone during several thousands of years and was filled by varved clays, coming mainly from the erosion of the Vercors and Dévoluy piedmonts. The clay deposits rest on either interglacial Riss–Würm period glaciofluvial materials (gravels and sands) or on underlying Jurassic carbonate bedrock which was folded and faulted during the alpine orogenesis. The thickness of the clay deposits can vary dramatically over a short distance, from 0 to a maximum of 200 m (Antoine et al., 1981), the clay top reaching maximum altitude of 750 m to 800 m. After sedimentation, the varved clays were partly covered by morainic terminal deposits brought by the rising of the Isère glacier at the end of the Würm period. This geological

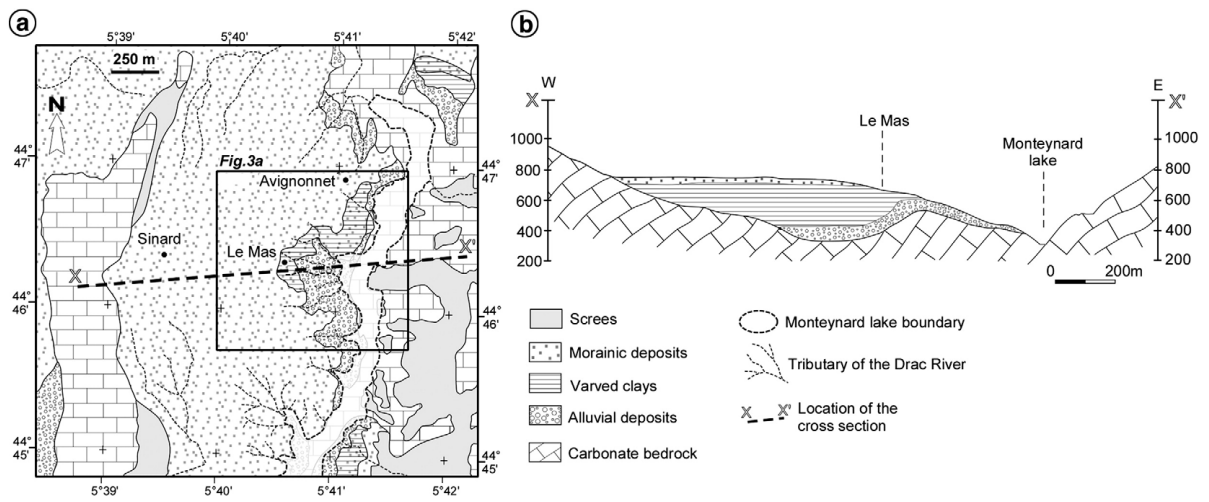


Fig. 2. a) Geological map and b) cross-section (XX') showing the structure of the region. The Avignonet landslide is within the rectangle (see Fig. 3a).

history explains the relatively flat depression of the Trièves region with clay outcropping over a large surface. After the glacier melting the rivers cut deeply into the geological formations and at least 15% of the area covered by the clay deposits is now considered as sliding. Some of these slides might affect surfaces as large as 500 000 m² with the deepest surface of rupture estimated or measured at about 40 m depth. The climate of the region is submediterranean with alpine influences and the activity of the landslides is generally seasonal with the largest displacement rates measured after snow melt and rain fall (Giraud et al., 1991; Van Asch et al., 1996). Most of these slides are moving slowly at a rate of a few cm/year or less (with local values as high as 1 m/year) but they might evolve into a mudflow with dramatic accelerations, as shown by the events of L'Harmallièrre (1981; Moulin and Robert, 2004) and of La Salle en Beaumont (1994, Moulin and Chapeau, 2004). During this last flow, four people were killed and 9

houses and the church of the village were seriously damaged or destroyed. The geological and geotechnical properties of the glaciolacustrine clays outcropping in the Trièves area were intensively studied in the eighties and summarized after more than 10 years of observations and geotechnical monitoring of several landslides (Giraud et al., 1991; Blanchet, 1988).

The Avignonet landslide is located east of the village of Sinard, along the Monteynard Lake (Fig. 2a). In this area, the thickness of the clay deposits varies from 0 to 200 m thick (Fig. 2b). They overlay either compact old alluvial deposits of the Drac river and/or marly limestone of Lias age. The alluvial deposits are made of a succession of cemented sand, gravel and pebble layers, overlaid with a level of blocky clay (Blanchet, 1988). The rocks outcrop on the eastern side of the lake and form the N–S orientated hill to the west of Sinard (Fig. 2a). The clays are covered by a thin layer (a few meters thick) of moraine material

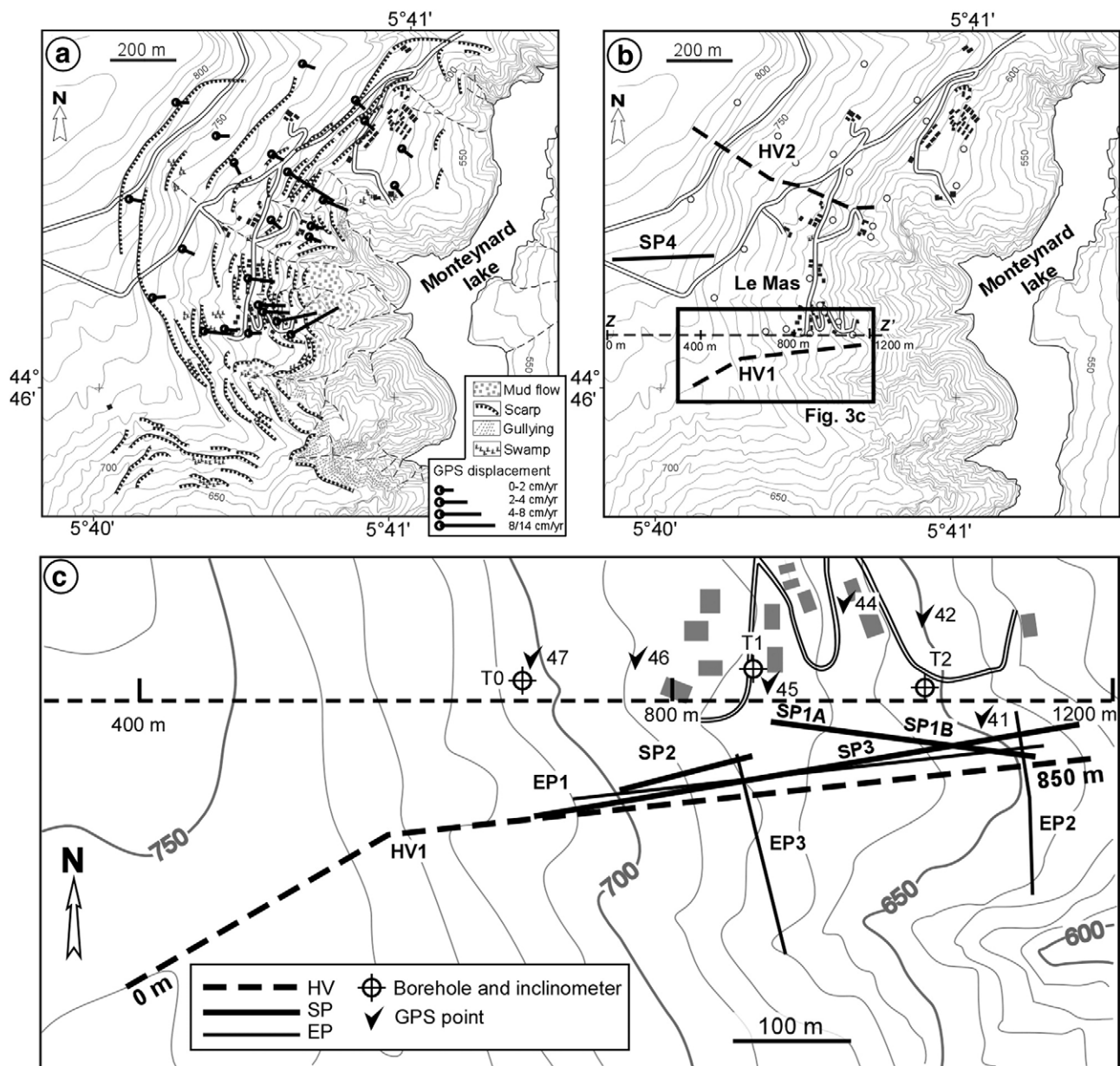


Fig. 3. a) Map of the Avignonet landslide with the location of the scarps and the displacement rates. b) The same with the location of the long geophysical profiles. The zone investigated in detail is indicated with a rectangle. Location of the geotechnical cross-section ZZ' is indicated. c) Map of the investigated zone with the location of the geophysical experiments, boreholes, inclinometers and GPS points. The HV:H/V profile. SP: Seismic Profile. EP: Electrical Profile. The geotechnical cross-section ZZ' is shown with dashed lines and the same abscissa as in Fig. 3b.

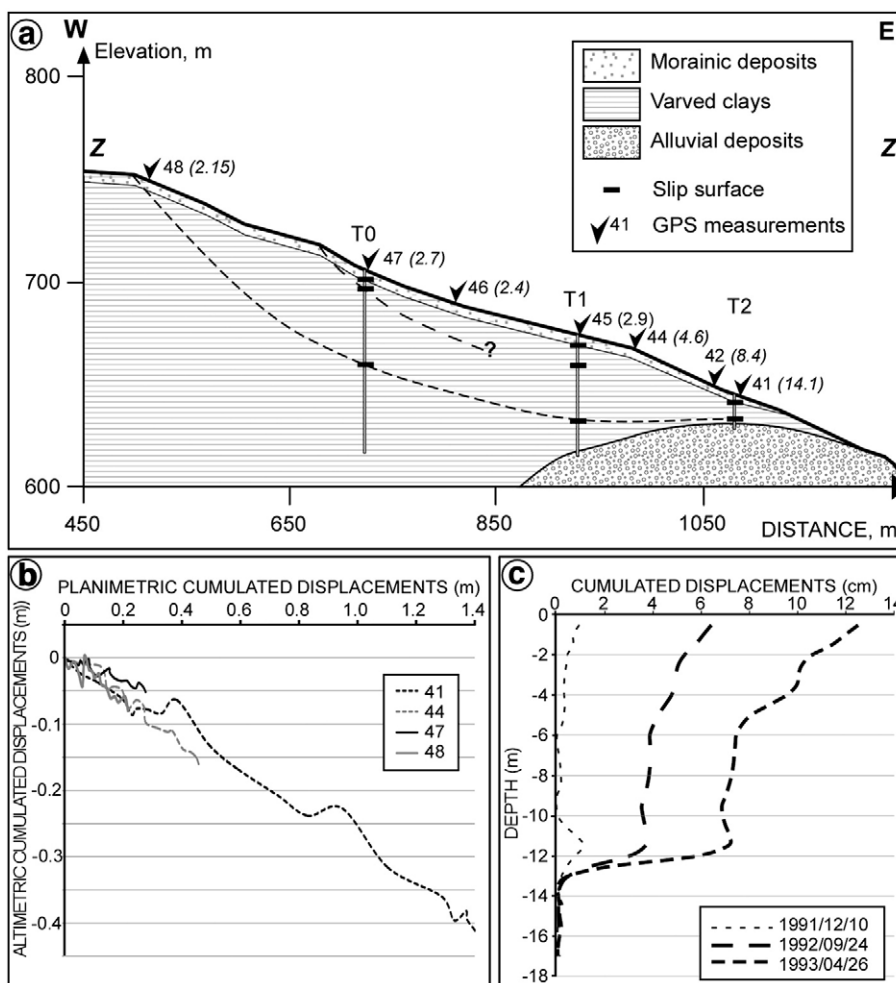


Fig. 4. a) Geotechnical cross section ZZ' (location in Fig. 3b) with the position of GPS points (displacement rate in cm/year are indicated between parentheses) and the slip planes deduced from inclinometer data in boreholes T0, T1 and T2. The vertical scale is exaggerated. Abscissa are the same as the ones in Fig. 3c b) Displacements in the horizontal and vertical planes at GPS points 41, 44, 47 and 48 (between 1995/10/01 and 2005/10/26). c) Cumulated displacements curve at inclinometer T2; reference curve was measured on 1990/04/10.

which are mixed up with displaced laminated clays on the slope, constituting a more permeable colluvial layer. The Avignonet slide affects a surface of about 1.10^6 m^2 (Fig. 3). The head scarp, which is approximately located at an elevation of 800 m, corresponds to the eastern border of the plateau (Figs. 2 and 3). Within the slide, the slope angle is between 8° and 15° and numerous signs of instability are found like scarps, fissures, gullies and mudflows (Fig. 3). Below the slide toe, the slope angle increases to 20° in the alluvial layers underlying the clay deposits.

The first signs of instability were noticed between 1976 and 1981, during housing development (Lorier and Desvarreux, 2004). Geotechnical investigation showed the existence of several slip surfaces, from very superficial ones (a few m) to deep ruptures at 40 m (Lorier and Desvarreux, 2004; Fig. 4a). The average slide velocity at the surface, measured by GPS during more than 10 years, increases downhill, varying from 0 to 2 cm/year at the top to more than 14 cm/year at the toe (Fig. 3a). These geodetic data are consistent with geomorphic observations (scarps, fissures, swampy areas, bulges), which show an increase of the landslide activity downstream. Piezometric data have pointed out a shallow water Table (1 m to a few m deep) which fluctuates with seasons. In case of heavy rainfalls or quick snow melt, this kind of slide might evolve into a mudflow, as shown by the events of L'Harmalière (1981) (Moulin and Robert, 2004) and of La Salle en Beaumont (1994) (Moulin and Chapeau, 2004), as well as by numerous solifluction flows.

A specific zone of the landslide was studied along the hamlet of Le Mas (Fig. 3) where geotechnical equipment (inclinometer) was placed in three boreholes (T0 to T2) and six fixed GPS points were available at the surface. Main results from geotechnical observation are summarized on the cross section ZZ' (Fig. 4). Location of the cross-section is shown in Fig. 3b. Boreholes T2 and T1 found the stiff alluvial layer at a depth of 14.5 m and 44.5 m, respectively, while T0 was stopped in the clay at 89 m, in agreement with the westward thickening of the clay deposit shown in Fig. 2a. Slip surfaces were detected in the three boreholes (Fig. 4a) at depths varying between a few m to 48 m. Fig. 4c shows the inclinometer data measured over 18 months in borehole T2 where the most active rupture surface is located at 13 m, over the clay–alluvium boundary. In T0 and T1, the maximum displacements

Table 1
S-wave velocity and density values considered within the layers for the computation of the resonance frequency.

| Geological unit | Vs (m/s) | Density |
|-------------------|----------|---------|
| Moraines | 250 | 1.9 |
| Disturbed clays | 300 | 2 |
| Varved clays | 650 | 2 |
| Alluvium | 1250 | 2 |
| Carbonate bedrock | 2000 | 2 |

See text for details.

were found at 4 and 48 m, respectively. Displacement rates at the surface strongly increase downhill, from 2 cm/year to 14 cm/year. The plots of the horizontal component versus the vertical component (Fig. 4b) show that the displacement vectors are roughly parallel to the slope, highlighting the translational character of the slide. Piezometric measurements (not shown) performed over 2 years in a hole close to GPS point 44 (Fig. 3c) indicate that the water table is about 2 m deep, with seasonal variations of about 1 m.

3. Geophysical investigation

Five methods (seismic noise measurement, electrical resistivity tomography, P-wave seismic refraction tomography, S-wave seismic refraction tomography and surface wave inversion) were used in the studied zone. The location of the different profiles is given in Fig. 3b and c.

3.1. Seismic noise measurements

Seismic noise measurements have been increasingly used in the last fifteen years in earthquake engineering for determining the geometry and shear wave velocity values of soil layers overlying bedrock (Wathelet et al., 2004; Bonnefoy-Claudet, 2006). The single

station method (also called the H/V technique) consists in calculating the horizontal to vertical spectral ratio of the noise records and allows the resonance frequency of the soft layer to be determined (Nakamura, 1989). For a single homogeneous soft layer, this fundamental frequency is given by $f_0 = V_s/4T$ where V_s is the soft layer shear wave velocity and T is the layer thickness. A description of the method is given by Bard (1998).

In this study, measurements of ambient vibrations were made every 50 m along two profiles (HV1 and HV2, Fig. 3b) using 5 s sensors. H/V spectral curves for profile HV1 are presented in Fig. 5a at two stations, as well as the H/V ratios for all the 18 stations as a function of frequency and distance in a greyscale. H/V curves at stations 3 and 15 both exhibit a well defined and single peak at 2 Hz and 0.6 Hz, respectively, with amplitude over 5. The H/V ratio map shows that the peak frequency regularly increases eastward, from about 0.5 Hz to 3.5 Hz. Considering the relation $f_0 = V_s/4T$, the evolution of the resonance frequency values is in agreement with the decrease of the clay thickness from 200 m to the West to about 20 m to the East.

Using the method of Kennett (2002), the resonance frequency below each station was computed from the 1D geometry and the properties of the geological layers (moraine, clay, alluvium and bedrock). Thickness values for each layer were obtained from the

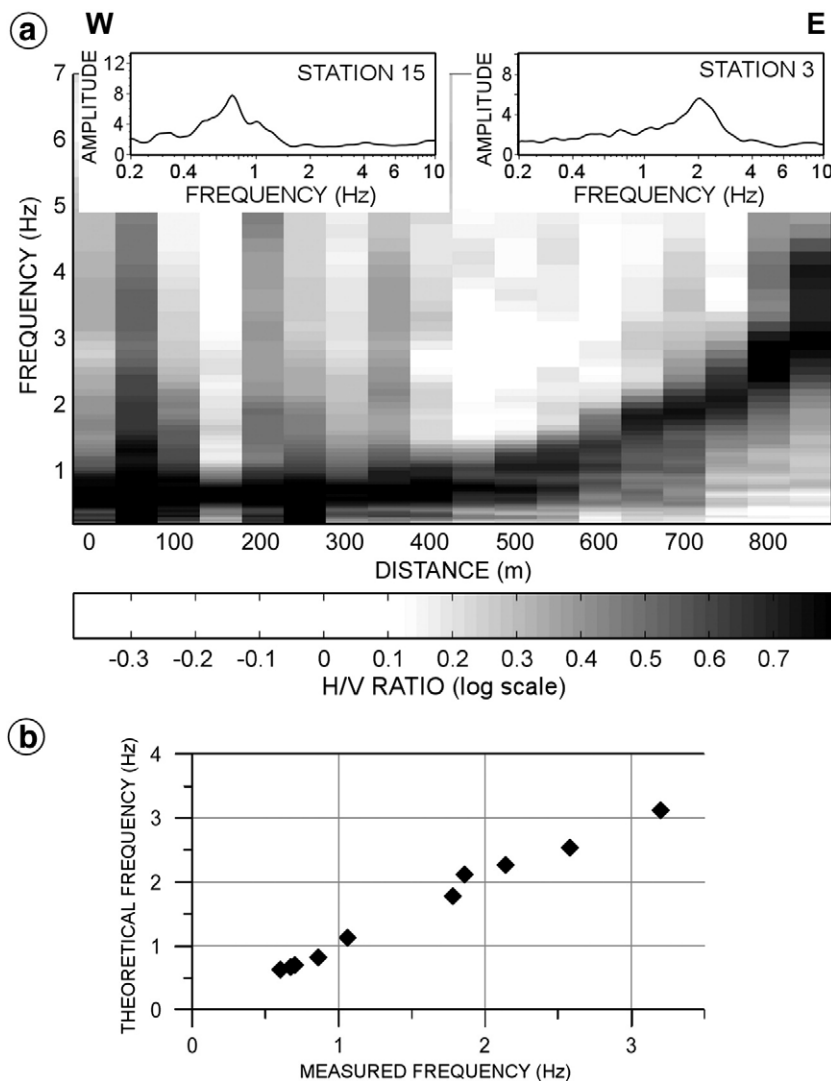


Fig. 5. a) H/V spectral ratio as a function of frequency and distance along profile HV1 (see Fig. 3b for location). H/V curves are plotted for stations 03 (750 m) and 15 (150 m). b) Plot of the theoretical resonance frequency as a function of the measured one. Parameters used for theoretical frequency calculation are presented in Table 1.

cross-section shown in Fig. 2b and a disturbed level of 5 m thickness was considered at the top of the clay layer. The considered characteristics (shear wave velocity V_s and density) of the layers are given in Table 1. V_s values in the shallow layers were obtained from our study in the shallow layers (see below), from previous seismic refraction tests (Blanchet, 1988) and from the results of a cross-hole test performed in the same formations (Méneroud et al., 1995). Theoretical and experimental values of the resonance frequency f_0 are compared in Fig. 5b and show a very good agreement. Sensitivity tests have shown that the main factor controlling f_0 is the total clay thickness. On the contrary, no change in the f_0 value is found when passing the landslide top. The same results were obtained for profile HV2, indicating that the H/V method is a robust tool for determining soft deposit thickness, as already observed by several authors (e.g. Delgado et al., 2000). In the Trièves area, this method can then be used for mapping the clay thickness variations, which is one of the major information for understanding landslide distribution.

3.2. Electrical Resistivity Tomography

Electrical resistivity methods are based on measuring the electrical potentials between one electrode pair while transmitting a direct current between another electrode pair (Reynolds, 1997). In Electrical Resistivity Tomography (ERT), a large number of electrodes and combinations of electrode pairs are used, providing a 2D image of electrical resistivity. Three electrical profiles (labelled EP1 to EP3) were conducted on the site, using the Wenner configuration. Their locations are given in Fig. 3c. Profile EP1, striking EW, was performed downslope with 64 electrodes 5 m apart, while EP2 and EP3 were made perpendicular to the slope with 64 electrodes spaced by 2.5 m. Electrical data were inverted with the algorithm developed by Loke and Barker (1996) and electrical images are shown in Fig. 6. All of them were obtained after a maximum of 5 iterations for misfit values lower than 3%. The three profiles were acquired in autumn at the end of the dry period. All profiles show a more or less continuous shallow

resistive layer (resistivity over 60 Ω m) with a thickness of a few meters. This corresponds to the colluvium made up of a mixing of moraines and clay above the water table. Below the water table, resistivity values are usually lower (between 10 and 40 Ω m) corresponding to the saturated varved clays. Resistive levels (over 60 Ω m) are detected at depth in the eastern part of the EP1 profile and at about 18 m depth below the EP2 profile. These resistive levels could correspond to the top (blocky clay) of the alluvial layers which were found at 14.5 m in borehole T2. The third electrical profile EP3, which crosses a highly deformed zone at its southern end (from 0 to 70 m), pointed out a relatively homogeneous conductive structure below the surficial resistive layer. Even if some weak lateral resistivity variations are observed in the clay deposits for all profiles, which are probably linked to water content changes, no clear relation was found between electrical resistivity lateral variations and the zones deformed by the landslide. Particularly, along EP1 (Fig. 6a), resistivity values do not show a correlation with the slide velocity values which increase between T1 and T2. In such saturated, soft and conductive material, our interpretation is that gravitational deformation does not change significantly the resistivity values which are already low, contrary to what was observed in compact shale and marl where degradation allowed the water content to be increased (Caris and van Asch, 1991; Lapenna et al., 2005).

3.3. P-wave refraction tomography

First arrivals in the seismic signals are inverted to get an image of the P-wave velocity distribution in the ground, assuming that the velocity increases with depth (Kearey et al., 2000). For this study, two 470 m long profiles (SP4 and SP3, Fig. 3b and c, respectively) were conducted with 48 vertical geophones (resonance frequency 4.5 Hz) spaced by 10 m. The signals were generated by 9 and 14 explosive sources with a spacing of 80 m and 50 m, respectively, including 1 to 2 offset shots at each end, depending on the accessibility of the area. Three other 115 m long profiles (SP1A, SP1B and SP2, Fig. 3c) were also

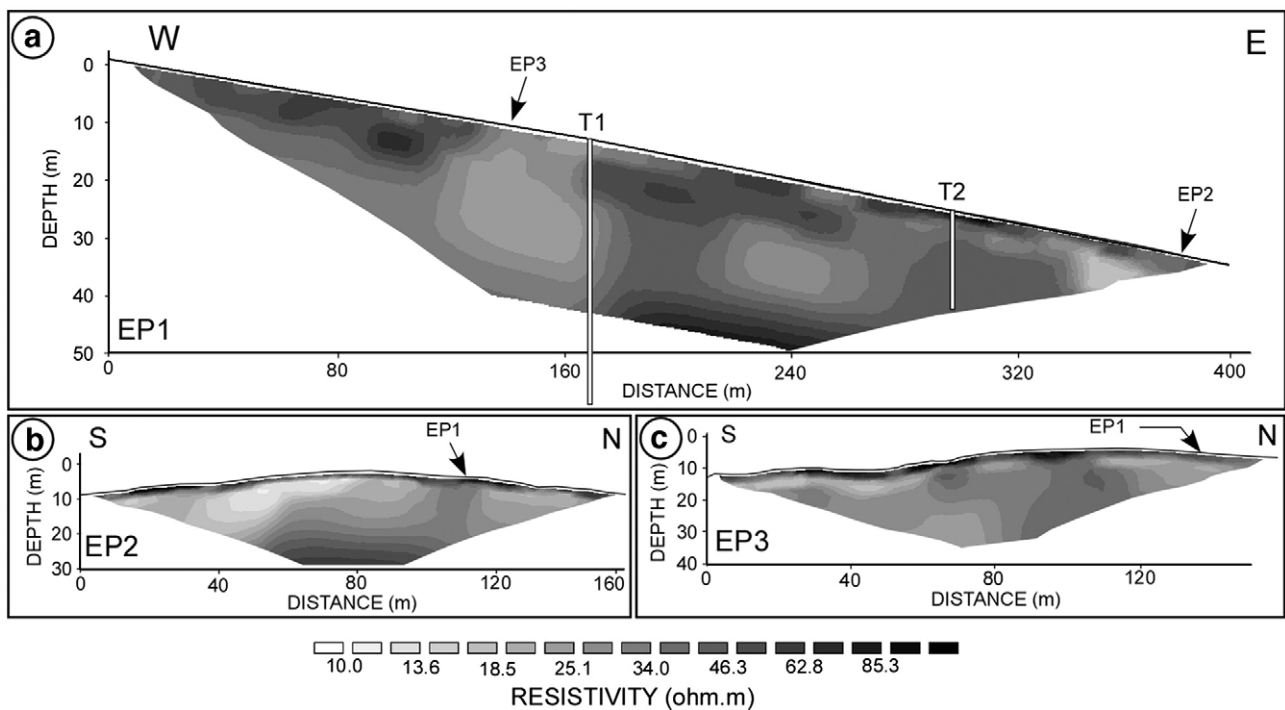


Fig. 6. Electrical profiles EP1 to EP3. a) Profile EP1 with 64 electrodes separated by 5 m; final misfit value is 1.6% after 5 iterations. Boreholes T1 and T2 are indicated. b) Profile EP2 with 64 electrodes separated by 2.5 m; final misfit value is 2.4% after 5 iterations. c) Profile EP3 with 64 electrodes separated by 2.5 m; final misfit value is 2.8% after 3 iterations.

carried out with 24 vertical geophones (resonance frequency 4.5 Hz) spaced by 5 m. Fig. 7a shows the seismograms recorded along profile SP4 for an offset shot at –85 m. One can easily distinguish the P-waves from the surface waves (Rayleigh waves). 207 and 322 first arrival times, clearly visible on the data, were picked for all shots on SP4 and SP3 respectively, with an uncertainty estimated around 0.5 ms. The time–distance graphs for three of them are plot in Fig. 7b. Below a thin surficial layer with a low velocity (less than 500 m/s), the clay deposits appear to be characterized by a very constant velocity around 1900 m/s.

The first-arrival times were inverted using the Simultaneous Iterative Reconstruction Technique (SIRT; Dines and Lyttle, 1979). The grid had cell sizes of 9 × 9 m and the two-layer starting model was derived from the classical interpretation of the graphs of Fig. 7b. Seismic images for profiles SP4 and SP3 are given in Fig. 7c and d, respectively. A misfit value lower than 1% was obtained in both cases after 3 iterations. Both profiles show a sharp vertical gradient in velocity, from a value lower than 1000 m/s near the surface to 1600–1800 m/s at less than 10 m depth. The first seismic layer corresponds to the moraine deposits and the unsaturated clay, while the second layer, whose velocity increases slightly with depth, can be associated with the saturated clay. Profile SP4 crosses the landslide limit (between 270 m and 300 m) and no significant P-wave lateral velocity variation is visible in Fig. 7c. Also, although the ground is much more deformed in the lower part of SP3, the seismic image of Fig. 7d does not show any lateral change. P-wave velocity in this case seems to be mainly controlled by the water level and little affected by the gravitational deformation. Similar results were obtained along the shorter profiles SP1 and SP2.

3.4. S-wave velocity measurements

Shear wave velocity (V_s) can be measured by various methods including active source techniques (borehole tests, SH refraction tests, surface wave inversion) and ambient vibration techniques (Jongmans, 1992; Tokimatsu, 1997; Socco and Jongmans, 2004). In this study we applied the SH seismic refraction method and the surface wave (SW) inversion for deriving V_s values along the cross-section ZZ' (Fig. 3b).

Surface waves (Rayleigh waves in this case), which are generated by vertical hammer drops, are dispersive, i.e. that their phase velocity C varies with the frequency f (Socco and Strobbia, 2004). At high frequency, the dispersion curve (Cf) is controlled by the shear wave velocity in the shallow layer while at low frequency it depends on V_s values in the deep layers. The dispersion curve can then be inverted to derive the shear wave velocity profile versus depth $V_s(z)$. An advantage of this method is that Rayleigh waves are recorded together with P-wave refraction, if a sufficient time length recording is considered during the acquisition. However, inversion of surface waves is theoretically limited to 1D velocity structures, although some smooth variations can be considered using the MASW technique (Park et al., 1999; Grandjean and Bitri, 2006). In the context of landslides, significant lateral V_s variations are expected in the highly deformed zones and the inversion of surface waves might be unusable. On the contrary, the SH refraction technique yields V_s 2D images, using the same algorithm (SIRT) as for P-waves. Both methods suffer the non uniqueness problem (Wathelet et al., 2004; Ivanov et al., 2006) and have to be constrained. In this study, we imposed the same solutions for the two data sets in the overlapping parts of the surveys. Dispersion curves for the fundamental mode of Rayleigh waves were computed using the $f-k$ method and inverted applying the Neighbourhood Algorithm (Socco and Strobbia, 2004; Wathelet et al., 2004).

The two long seismic profiles SP3 and SP4 were used to study the Rayleigh wave propagation along the sliding mass. Groups of geophones located in regions with roughly homogenous 1D media were selected from the seismogram examination and the P-wave images: 3 groups along SP4 (A: 1–15, B: 19–30, C: 38–48; Fig. 7a) and 4 groups along SP3 (A: 1–9, B: 9–28, C: 29–35, D: 35–44, Fig. 7d). The results of the SW inversion for the two groups SP4A and SP4C are presented in Fig. 8. Profile SP4 was performed across the landslide limit which is located between 270 m and 300 m (Fig. 7a). Dispersion curves were computed for the two offset shots (direct and reverse) in order to test the 1D hypothesis and the average of the two curves was computed (Fig. 8a and b). Within the landslide (Fig. 8b), the Rayleigh wave curve exhibits lower velocity values than in the undisturbed area (Fig. 8a), over the whole frequency range. Dispersion curves are

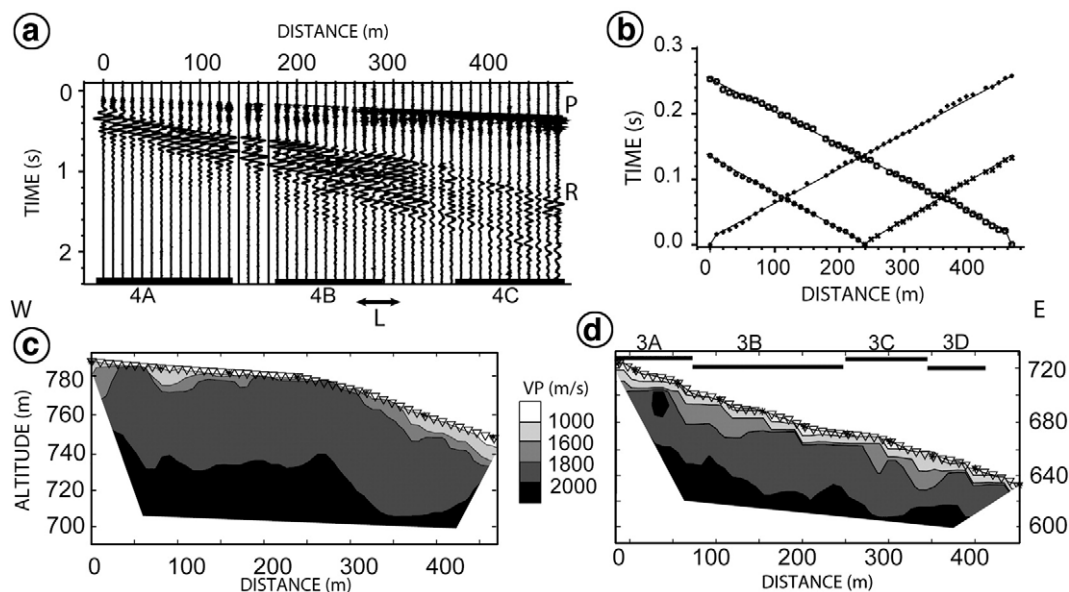


Fig. 7. P-wave refraction study. a) Seismograms recorded along profile SP4 for an offset shot at –85 m. P: P-waves, R: Rayleigh waves. Bold bars labelled 4A to 4C locate the groups of geophones used for the surface wave inversion, double arrow L indicates the location of the landslide top. b) Travel-time versus distance graphs for the three shots at 0 m, 250 m and 470 m along SP4. c) and d) P-wave velocity images along profiles SP4 and SP3, respectively. The initial model for the inversion is a 9 m thick layer ($V_p = 500$ and 650 m/s, respectively) over a half space ($V_p = 2500$ m/s). Bold bars labelled 3A to 3D locate the groups of geophones used for the surface wave inversion.

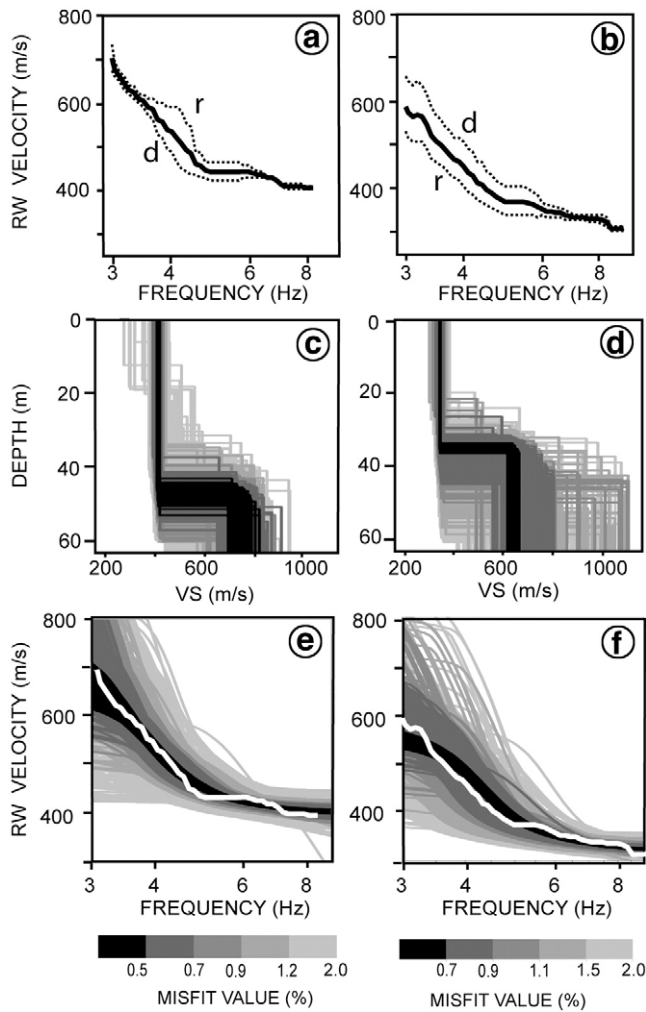


Fig. 8. Surface wave inversion (Rayleigh waves, fundamental mode) performed on 2 groups of seismograms along profile SP4. Left column: group SP4A. Right column: group SP4C. a) and b) Dispersion curves for direct (d) and reverse (r) shots with offset. The black line corresponds to their average. c) and d) Vs profiles resulting from the inversion of these dispersion curves. e) and f) Corresponding calculated dispersion curves with the average experimental data. Models and dispersion curves are plotted with a misfit greyscale.

inverted assuming the simplest parameterisation with a two layer model (Fig. 8c and d), which will be justified in the next section. Out of the landslide, Fig. 8 shows that Vs velocity in the upper 45–50 m thick layer is about 400 m/s and decreases slightly to less than 350 m/s within the slide.

Fig. 9 shows the phase velocity dispersion curves computed, for each of the seven groups of geophones (profiles SP3 and SP4), from the average of all coherent dispersion curves calculated from the different shots. They present a common frequency range between 3 and 13 Hz. The striking feature is that, in the high frequency range (over 8 Hz), Rayleigh wave velocities regularly decrease from the top (SP4A) to the bottom of the hill (SP3D), with the exception of SP3C. Although profiles SP3 and SP4 are separated some hundred meters apart from each other in N–S direction, the behaviour of the slope instability does not seem to change much over this distance. Phase velocity values at 10 Hz are divided by 2, from 400 m/s out of the landslide to 200 m/s in the most deformed zones. The lower frequencies do not show a similar phase velocity decrease along the profile because they sample in the bottom part the compact underlying alluvial deposits characterized by much higher velocities (see, for instance the curve SP3D). The seven dispersion curves were inverted using the Neighbourhood Algorithm

(Wathelet et al., 2004), with two different parameterisations: a simple two layer model, and a two layer model with a linear Vs increase within the top layer. On the basis of the combined analysis together with SH refraction, the simple two layer model was selected and the results will be discussed in the following section.

Regarding the SH wave refraction technique, three 115 m long profiles were performed at the same place as the short P-waves profiles (SP1A, SP1B, SP2; Fig. 3c). SH waves were generated by hitting a weighted plank oriented perpendicular to the profile direction and recorded by 24 horizontal 14 Hz geophones. Seismograms were recorded for 13, 7 and 11 SH sources regularly spaced along SP1A, SP1B and SP2 respectively (i.e. with 10 m, 20 m and 15 m source spacing). Fig. 10a shows the seismograms recorded for an end shot along profile SP1A, while the travel-time versus distance graphs are presented in Fig. 10b for the two extreme shots. The uncertainty on these arrival times is estimated around 2 ms. Compared to P-waves, SH arrival time graphs exhibit a more complex shape, with both vertical and horizontal variations of apparent Vs values which range from 220 m/s to 730 m/s. SH wave times were picked and the 299, 161 and 253 travel-times measured along the seismic profiles SP1A, SP1B and SP2, respectively, were inverted using the SIRT technique with a 4 m side cell grid and different starting models. Fig. 10c and d show the Vs images obtained for the two profiles SP1A and SP1B, that explain both the SH wave and the surface wave data at the same place. The ray coverage is added in Fig. 10e and f, delimiting the reliable parts of the seismic section. SH-wave images exhibit a thick low-velocity layer (Vs about 250 m/s) overlying a more compact layer (Vs > 600 m/s) found at a depth varying between 20 m from the top to 12 m at the bottom of the profile. This range is consistent with the depth of the slip surface (13 m) detected in T2 (Fig. 4c). The low Vs values measured above the slip surface probably result from the cracking of the clay which increases the porosity at the wavelength scale (a few m to 10 m). Moreover, the Vs image of profile SP1B shows a lateral velocity decay (from 250 m/s to 200 m/s) in the top layer towards the bottom of the profile, which coincides with the slide velocity increase. This point will be discussed in the next section.

4. Discussion and conclusion

Vs measurements for all profiles are summarized in Fig. 11, along the cross-section ZZ'. For comparison, Vs values measured on the plateau at 800 m from the slide top are also plotted, along with the

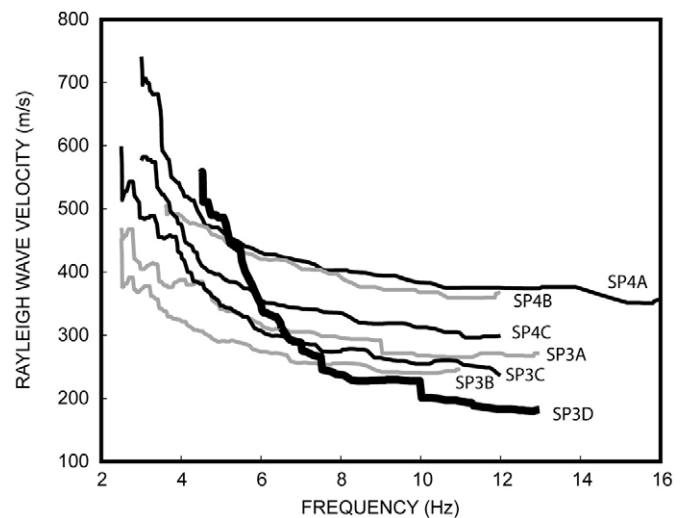


Fig. 9. Comparison of the dispersion curves calculated along the landslide. SP4A to C correspond to geophones 1–15, 19–30 and 38–48, respectively. SP3A to D correspond to geophones 1–9, 9–28, 29–35 and 35–44, respectively.

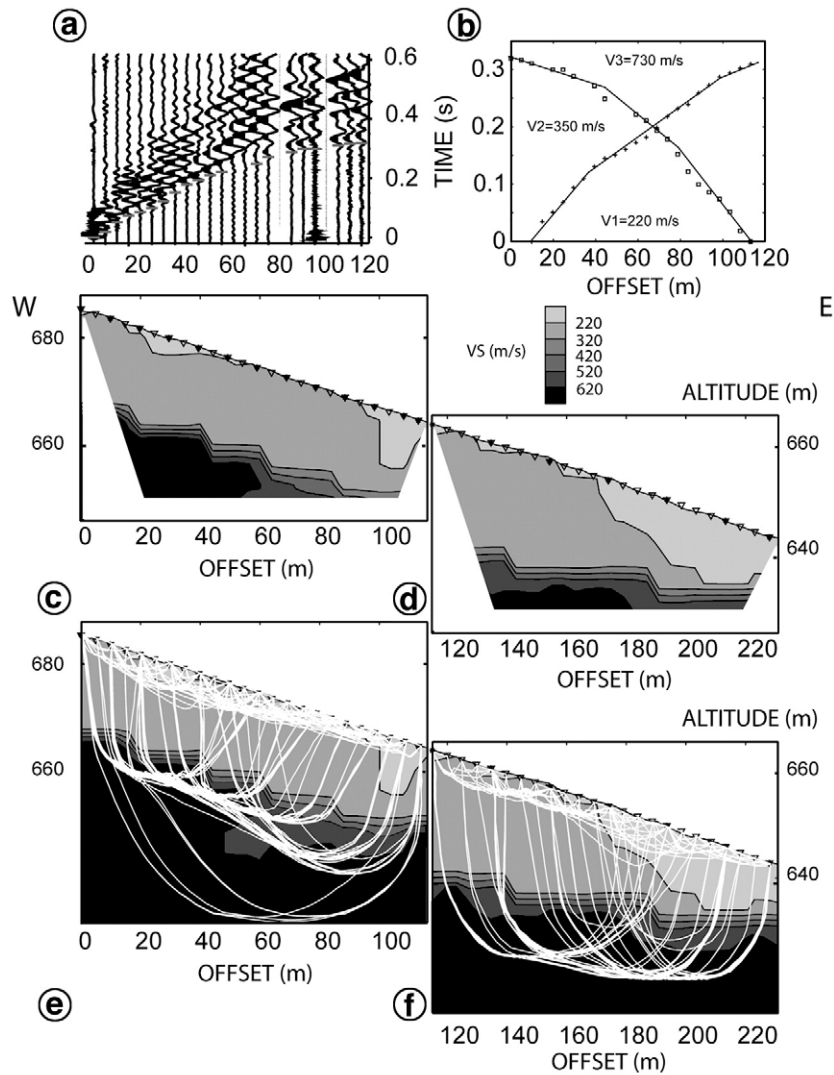


Fig. 10. SH wave refraction study. a) Seismograms recorded along profile SP1A for a shot at 0 m. b) Traveltime-distance graphs for the 2 shots at 15 m and 115 m along profile SP1A. c) and d) SH-wave velocity images for profiles SP1A and SP1B, respectively. Misfit values are lower than 2.5%. The initial model is a 20 m thick layer ($V_s = 250$ m/s) over a half space ($V_s = 800$ m/s).

value of V_s obtained at 25 m depth by a cross-hole test for a bridge investigation (Ménéroud et al., 1995). In Fig. 11b are plotted V_s values (measured by the two methods) versus distance at a depth of 5 m, together with the slide velocity measurements. The striking feature is the regular decay of V_s values along the section, from 500 m/s far from the slide to 200 m/s at the slide toe. Within the slide, the V_s variation is opposite to the slide velocity curve, suggesting that the gravitational deformation strongly affects the shear wave velocity within the clay, contrary to what was observed for P-wave velocity and electrical resistivity. V_s values averaged at 25 m depth are shown in Fig. 11c. In the western part of the section, V_s values at 25 m exhibit the same decrease as at 5 m. On the contrary, V_s values are higher (500–600 m/s) at the slide toe than over the head scarp (400 m/s), resulting from the presence of the stiff shallow alluvial layers. In the transition zone (between 750 m and 950 m of distance) the depth of the interface separating the first and second seismic layer is close to 25 m and V_s values in both layers are plotted, showing the gradual lateral variation. Two independent measurements made far from the slide at 25 m depth (star and square in Fig. 11c) show V_s values higher (600–650 m/s) than the ones measured near the head scarp. These results, along with the values measured at 5 m depth and the weak displacement rates measured by the GPS point located beyond the head scarp, suggest that the clay mass at the rear has already been degraded over a distance of a few hundreds

meters by a slow motion along a deep slip surface (about 40 m deep). V_s values measured on the Avignonet site (from 200 m/s to 600 m/s) are in a range similar to the one obtained by Mondol et al. (2007) in saturated marine clay for vertical effective stresses between 5 and 40 MPa, corresponding to burial depths from a few hundreds of meters to a few kilometres. This difference of depths is probably due to the over-consolidation of the laminated clay resulting from the action of the glacier, as well as to the silty component of the material. This comparison nevertheless illustrates the significant effect of the slide on the V_s values, with a division by a factor of 2.5 between the zones unaffected and strongly deformed by the landslide. This decay probably results from the decompaction and intensive cracking at different scales of the laminated clay.

All these results suggest that, unlike V_p or electrical resistivity values that are mainly driven by water content in such saturated clay, V_s mapping could provide valuable information on the deformation state of the clay material at depth, and that V_s evolution with time could be used as an indicator for characterizing the landslide activity. If the slide evolves into a flow, V_s should even tend to zero in the zones behaving as a fluid. The methods as well as the corresponding layouts and instruments used in this study for determining V_s are limited to a penetration depth between 25 m and 40 m. In the future, an effort should be made to develop V_s

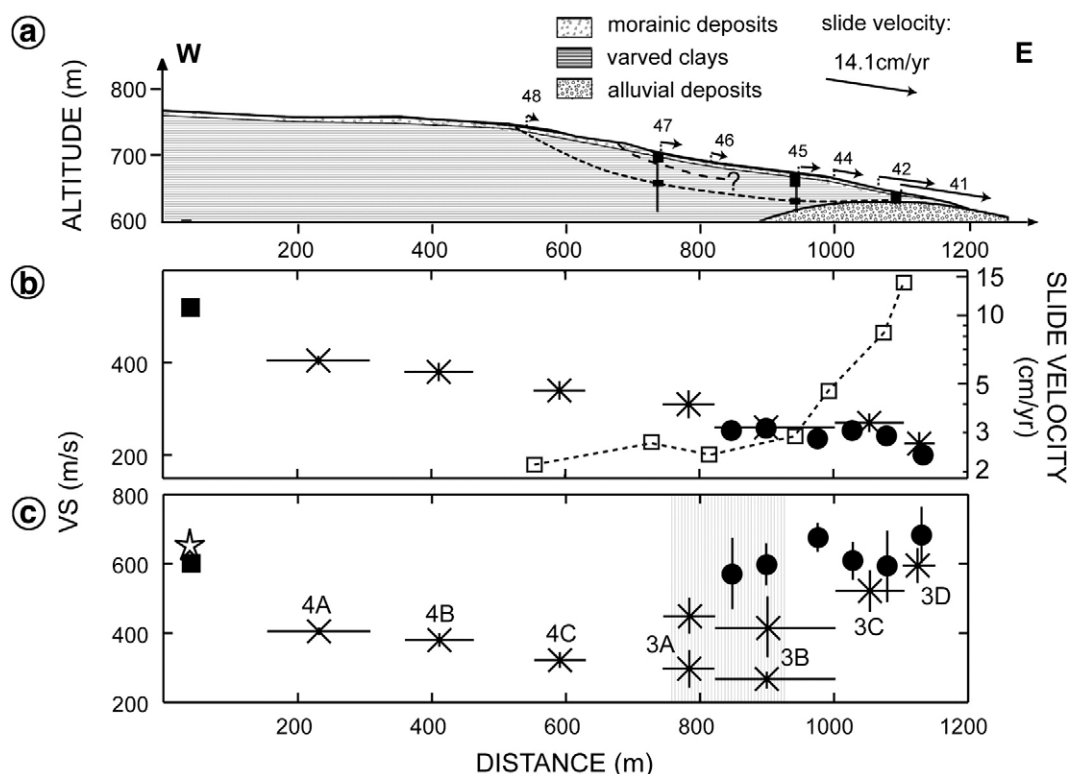


Fig. 11. a) Geotechnical cross-section ZZ' with the arrows of the slide velocity. b) and c) Vs values at 5 m and 25 m depth as a function of distance with vertical error bars. Crosses: Vs values deduced from SW inversion, with horizontal bars indicating the distance range. Dots: Vs values from SH wave refraction. Square: Vs values measured from SH refraction tests at 800 m from the slide limit on the plateau. Star: Vs value measured in a remote cross-hole test. Seismic profiles SP4A to C and SP3A to D, are labelled 4A to 4C and 3A to 3D, respectively. In Figure b are plotted the slide velocity values. The grey area in Figure c corresponds to the transition zone where the depth of the interface separating the first and second seismic layer is close to 25 m and Vs values in both layers are plotted.

measurement techniques which are repetitive and reliable at greater depth. The recent application of cross-correlation techniques on the seismic noise recorded by permanent seismic stations (Larose et al., 2006) offers Vs imaging possibilities which should be tested on landslides in the future. Also, an effort should be made to understand relation between cracking and Vs values through laboratory tests on clay samples.

Acknowledgments

This work was financially supported by European, regional and national funds coming from the Mountain Risks project (Marie Curie program), the Conseil Général de l'Isère, the region Rhône-Alpes, the ECOUPREF project and the Cluster VOR (Vulnérabilité des Ouvrages aux Risques). The authors thank all the people who participated to the field investigation, as well as RTM (Restauration des Terrains en Montagne) and SAGE (Société Alpine de Géotechnique) for providing the geotechnical data. We thank Th. W. J. van Asch and an anonymous reviewer for their helpful comments.

References

- Antoine, P., Giraud, A., Monjuvent, G., 1981. Les argiles litées du Trièves (Isère): conditions de gisement et exemples de propriétés géotechniques. *Bulletin de la société géologique de France* 23, 117–127.
- Archie, G.E., 1942. The electrical resistivity log as an aid in determining some reservoir characteristics. *Petroleum Technology* 1, 55–62.
- Bard, P.-Y., 1998. Microtremor measurements: a tool for site effect estimation? *Proceeding of the Second International Symposium on the Effects of Surface Geology on Seismic Motion*, Yokohama, Japan, 3, 1251–1279.
- Blanchet, F., 1988. Etude géomécanique de glissements de terrain dans les argiles glaciolacustres de la vallée du Drac. Ph.D. thesis, Grenoble university, 157 p.
- Bogoslovsky, V.A., Ogilvy, A.A., 1977. Geophysical methods for the investigation of landslides. *Geophysics* 42, 562–571.

- Bonnefoy-Claudet, S., Cornou, C., Bard, P.-Y., Cotton, F., Moczo, P., Kristek, J., Fäh, D., 2006. H/V ratio: a tool for site effects evaluation. Results from 1-D noise simulation. *Geophysical Journal International* 167, 827–837.
- Caris, J.P.T., van Asch, T.W.J., 1991. Geophysical, geotechnical and hydrological investigations of a small landslide in the French Alps. *Engineering Geology* 31 (3–4), 249–276.
- Delgado, J., Lopez Casado, C., Estevez, A., Giner, J., Cuenca, A., Molina, S., 2000. Mapping soft soils in the Segura River valley (SE Spain): a case of study of microtremors as an exploration tool. *Journal of Applied Geophysics* 45, 19–32.
- Dines, K., Lytle, J., 1979. Computerized geophysical tomography. *Proceedings of the Institute of Electrical and Electronics Engineers* 67, 1065–1073.
- Gallipoli, M., Lapenna, V., Lorenzo, P., Mucciarelli, M., Perrone, A., Piscitelli, S., Sdao, F., 2000. Comparison of geological and geophysical prospecting techniques in the study of a landslide in southern Italy. *European Journal of Environmental and Engineering Geophysics* 4, 117–128.
- Giraud, A., Antoine, P., van Asch, T.W.J., Nieuwenhuis, J.D., 1991. Geotechnical problems caused by glaciolacustrine clays in the French Alps. *Engineering Geology* 31, 185–195.
- Guillier, B., Cornou, C., Kristek, J., Bonnefoy-Claudet, S., Bard, P.-Y., Faeh, D., and Moczo, P., 2006. Simulation of seismic ambient vibrations: does the H/V provide quantitative information in 2D–3D structure. *ESG2006*, Grenoble.
- Grandjean, G., Bitri, A., 2006. 2M-SASW: multifold multichannel seismic inversion of local dispersion of Rayleigh waves in laterally heterogeneous subsurfaces: application to the Super Sauze earthflow, France. *Near Surface Geophysics* 4, 367–375.
- Grandjean, G., Pennetier, C., Bitri, A., Méric, O., Malet, J.P., 2006. Caractérisation de la structure interne et de l'état hydrique de glissements argilo-marneux par tomographie géophysique: l'exemple du glissement-coulée de Super-Sauze. *Comptes Rendus Geosciences* 338 (9), 587–595.
- Ivanov, I., Miller, R.D., Xia, J., Steeples, D., Park, C.B., 2006. Joint analysis of refractions with surface waves: an inverse solution to the refraction-traveltime problem. *Geophysics* 71 (6), R131–R138.
- Jongmans, D., 1992. The application of seismic methods for dynamic characterization of soils in earthquake engineering. *Bulletin of the International Association of Engineering Geology* 46, 63–69.
- Jongmans, D., Garambois, S., 2007. Geophysical investigation of landslides: a review. *Bulletin Société Géologique de France* 178, 2.
- Kearey, P., Brooks, M., Hill, I., 2000. *An Introduction to Geophysical Exploration*. Blackwell Science, 264 pp.
- Kennett, B.L.N., 2002. *The Seismic Wavefield: Vol. 1: Introduction and Theoretical Development*. Cambridge University Press, Cambridge, p. 368.
- Lapenna, V., Lorenzo, P., Perrone, A., Piscitelli, S., Rizzo, E., Sdao, F., 2005. 2D electrical resistivity imaging of some complex landslides in Lucanian Apennine chain, southern Italy. *Geophysics* 70, B11–B18.

- Larose, E., Margerin, L., Derode, A., van Tiggelen, B., Campillo, M., Shapiro, N., Paul, A., Stehly, L., Tanter, M., 2006. Correlation of random wave fields: an interdisciplinary review. *Geophysics* 71, S111–S121.
- Leucci, G., De Giorgi, L., 2006. Experimental studies on the effects of fracture on the P and S wave velocity propagation in sedimentary rock ("calcarene del Salento"). *Engineering Geology* 84, 130–142.
- Lorier, L., and Desvarreux, P., 2004. Glissement du Mas d'Avignonet, commune d'Avignonet: Proceedings of the workshop Ryskhydrogeo, Program Interreg III, La Mure (France), 8p.
- Loke, M.H., Barker, R.D., 1996. Rapid least-squares inversion of apparent resistivity pseudosections using a quasi-Newton method. *Geophysical Prospecting* 44, 131–152.
- McCann, D.M., Forster, A., 1990. Reconnaissance geophysical methods in landslide investigations. *Engineering Geology* 29, 59–78.
- Méric, O., Garambois, S., Cadet, H., Malet, J. -P., Guéguen, P., and Jongmans, D., 2007. Seismic noise based methods for soil landslide characterization, *Bulletin Société Géologique de France*, 178, n°2.
- Mavko, G., Mukerji, T., Dvorkin, J., 2003. *The Rock Physics Handbook, Tools for Seismic Analysis of Porous Media*. Cambridge University Press, Cambridge, 339 p.
- Méneroud, J.-P., Duval, A.-M., Vidal, S., Fréchet, J., Gamond, J.-F., Beck, C., Tardy, M., Bard, P.-Y., Barnichon, E., and Gaboriaud, J.-M., 1995. A51 Grenoble – Sisteron, Franchissement de l'Ebron, Etude de l'aléa sismique local: internal report CETE Méditerranée, n°93/95666/74, 176 p.
- Mondol, N.H., Bjorlykke, K., Jahren, J., Hoeg, K., 2007. Experimental mechanical compaction of clay mineral aggregates – changes in physical properties of mudstones during burial. *Marine and Petroleum Geology* 24, 289–311.
- Moulin, C., and Chapeau, C., 2004. Le glissement de la Salle en Beaumont (Isère), Proceedings of the workshop Ryskhydrogeo, Program Interreg III, La Mure (France), 9 p.
- Moulin, C., and Robert, Y., 2004. Le glissement de l'Harmalière sur la commune de Sinard: Proceedings of the workshop Ryskhydrogeo, Program Interreg III, La Mure (France), 11 p.
- Monjuvent, G., 1973. La transfluence Durance-Isère. Essais de synthèse du Quaternaire du bassin du Drac. *Géologie Alpine* 49, 57–118.
- Nakamura, Y., 1989. A method for dynamic characteristics estimation of subsurface using microtremor on ground surface. *QR of RTRI* 30, 25–33.
- Park, C.B., Miller, R.D., Xia, J., 1999. Multi-channel analysis of surface waves. *Geophysics* 64 (3), 800–808.
- Picarelli, L., 2000. Mechanisms and Rates of Slope Movements in Fine Grained Soils. *Int Conf Geotech Geol Eng GeoEng 2000*, vol. 1, pp. 1618–1670.
- Picarelli, L., Urciuoli, G., Russo, C., 2004. The role of groundwater regime on behaviour of clayey slopes. *Canadian Geotechnical Journal* 41, 467–484.
- Reynolds, 1997. *An Introduction to Applied and Environmental Geophysics*. Wiley, 796 pp.
- Schmutz, M., Albouy, Y., Guerin, R., Maquaire, O., Vassal, J., Schott, J.J., Desclotres, M., 2000. Joint inversion applied to the Super Sauze earthflow (France). *Surveys in Geophysics* 21, 371–390.
- Socco, L.V., Jongmans, D., 2004. Special issue on seismic surface waves. *Near Surface Geophysics* 2, 163–258.
- Socco, L.V., Strobbia, C., 2004. Surface-wave method for near-surface characterization: a tutorial. *Near Surface Geophysics* 2, 165–185.
- Tokimatsu, K., 1997. Geotechnical site characterization using surface waves. In: Ishihara (Ed.), *Proc. 1st Intl. Conf. Earthquake Geotechnical Engineering*, Volume 3. Balkema, pp. 1333–1368.
- Van Asch, Th.W.J., Hendriks, M.R., Hessel, R., Rappange, F.E., 1996. Hydrological triggering conditions of landslides in varved clays in French Alps. *Engineering Geology* 42, 239–251.
- Wathelet, M., Jongmans, D., Ohrnberger, M., 2004. Surface wave inversion using a direct search algorithm and its application to ambient vibration measurements. *Near Surface Geophysics* 2, 211–221.
- Willye, M.R.J., Gregory, A.R., Gardner, L.W., 1956. Elastic wave velocities in heterogeneous and porous media. *Geophysics* 21, 41–70.